Probing a major DNA weakness: resolving the groove and sequence selectivity of the diimine complex Λ-[Ru(phen)2phi]2+

Prieto Otoya, T. D., McQuaid, K. T. ORCID: https://orcid.org/0000-0002-3222-5584, Hennessy, J., Menounou, G., Gibney, A., Paterson, N., Cardin, D. J., Kellett, A. and Cardin, C. J. ORCID: https://orcid.org/0000-0002-2556-9995 (2024) Probing a major DNA weakness: resolving the groove and sequence selectivity of the diimine complex Λ-[Ru(phen)2phi]2+. Angewandte Chemie International Edition, 63 (13). e202318863. ISSN 1521-3773 doi: 10.1002/anie.202318863 Available at https://centaur.reading.ac.uk/115088/

the End User Agreement.

www.reading.ac.uk/centaur

CentAUR

Central Archive at the University of Reading

Reading's research outputs online

DNA Grooves

Probing a Major DNA Weakness: Resolving the Groove and Sequence Selectivity of the Diimine Complex Λ-[Ru(phen)₂phi]²⁺

Tayler D. Prieto Otoya, Kane T. McQuaid, Joseph Hennessy, Georgia Menounou, Alex Gibney, Neil G. Paterson, David J. Cardin, Andrew Kellett,* and Christine J. Cardin*

Abstract: The grooves of DNA provide recognition sites for many nucleic acid binding proteins and anticancer drugs such as the covalently binding cisplatin. Here we report a crystal structure showing, for the first time, groove selectivity by an intercalating ruthenium complex. The complex Λ-[Ru(phen)₂phi]²⁺, where phi = 9,10-phenanthrenediimine, is bound to the DNA decamer duplex d(CCGGTACCGG)₂. The structure shows that the metal complex is symmetrically bound in the major groove at the central TA/TA step, and asymmetrically bound in the minor groove at the adjacent GG/CC steps. A third type of binding links the strands, in which each terminal cytosine base stacks with one phen ligand. The overall binding stoichiometry is four Ru complexes per duplex. Complementary biophysical measurements confirm the binding preference for the Λ-enantiomer and show a high affinity for TA/TA steps and, more generally, TA-rich sequences. A striking enantiospecific elevation of melting temperatures is found for oligonucleotides which include the TATA box sequence.

[*] T. D. Prieto Otoya, Dr. K. T. McQuaid, Prof. Dr. D. J. Cardin,
Prof. Dr. C. J. Cardin
Department of Chemistry, University of Reading, Whiteknights,
Reading, RG6 6AD, UK
E-mail: c.j.cardin@reading.ac.uk

Dr. J. Hennessy, Dr. G. Menounou, Dr. A. Gibney, Prof. Dr. A. Kellett
SSPC, the Science Foundation Ireland Research Centre for
Pharmaceuticals,
School of Chemical Sciences,
Dublin City University,
Glasnevin, Dublin 9, Ireland

Email :
E-mail: andrew.kellett@dcu.ie

Dr. N. G. Paterson
Diamond Light Source Ltd., Harwell Science and Innovation
Campus, Didcot, Oxfordshire, OX11 0DE, UK

Introduction

The DNA decamer sequence d(CCGGTACCGG) is remarkable in spontaneously crystallising in the X-stacked Holliday junction form.[1] The original serendipitous discovery was made while crystallising mismatched decamers, and the crystallised assembly had the structure predicted from solution studies.[2] A systematic study of all 64 self-complementary combinations of d(CCN1N2N3n3n2n1GG) then showed that the presence of ACC as the central triplet gave only the junction form under the deliberately restricted set of conditions used, whereas other triplets were amphimorphic or gave exclusively B-DNA or A-DNA.[3] In solution, this sequence is a mixture of duplex and junction forms.[4] We showed that the junction structure was maintained in the presence of other Group II divalent cations, including Sr²⁺ and Ba²⁺.[5–8] More surprisingly, our study of an anticancer bisacridine-4-carboxamide bound to the same junction structure showed the remarkably small changes in overall topology which resulted, with the central adenine base displaced, and replaced by the acridine chromophores.[9] A flexible linker was found crossing the major groove face of the junction, and this work remains the only structural characterisation of this binding mode. We have recently summarised the roles of junctions, and the therapeutic potential of junction-binding small molecules.[10]

Strikingly, when d(CCGGTACCGG) was crystallised with ruthenium polypyridyl complexes, we saw a quite different pattern of behaviour.[8,11] This decamer formed a kinked and intercalated B-DNA duplex. Our initial study used the closely related d(TCGGCGCCGA) sequence, which as the native can crystallise either as B-DNA or in the junction form, depending on the crystallisation conditions.[3] In the presence of Λ-[Ru(TAP)₂dppz]²⁺, (TAP = tetraazaphenanthrene) we found that the dppz chromophore intercalated at the terminal step, with one TAP ligand kinking the GG/CC step of an adjacent duplex in the crystal lattice.[8] With the d(CCGGTACCGG) sequence, and using the structurally isomorphous phen ligand, the combination of d(CCGGTACCGG) and Λ-[Ru(phen)₂dppz]²⁺ was then found to bind an additional complex by symmetrical intercalation at the central TA/TA step.[11] All these ruthenium complex intercalations and kinkings are from the minor groove of the duplex. This work highlighted the susceptibility of the TA/TA step in B-DNA to intercalation, which we ascribe to the weak stacking energy of this step.[12] A further consequence of the weakness is that it permits high local twisting of the duplex at this step.[11]

It was suggested many years ago that the use of triple helices could provide a way of specifically targeting DNA sequences for gene editing or silencing purposes.[13,14] The use of metal complexes in such applications is a more recent development,[15–17] and for precise molecular design, to minimise off-target effects, it is essential to use, as a component of such constructs, a metal complex whose binding modes are well understood.[18] And, as triplex forming oligonucleotides (TFOs) bind in the major groove via Hoogsteen (parallel) or reverse-Hoogsteen (anti-parallel) interactions, optimal selection of major groove binding metal complexes would be expected to maximise DNA reactivity. One approach would be to use a ruthenium polypyridyl complex which intercalates from the major groove, but as far as is known, there is no reported structural data which demonstrates such a binding mode.[19]

Here we report the crystal structure of Λ-[Ru-(phen)$_2$phi]$^{2+}$ (phi=9,10-phenanthrenediimine) with the DNA sequence d(CCGGTACCGG). As outlined above, this is the same sequence used in our previous report of the binding modes of Λ-[Ru(phen)$_2$dppz]$^{2+}$.[11] In that work we reported the three binding modes outlined above. Now we report a directly comparable structure, and observe the Λ-[Ru(phen)$_2$phi]$^{2+}$ complex symmetrically intercalated from the major groove at the TA/TA step, with angled (canted) binding at the adjacent GG/CC step, and a third Ru complex linking the duplexes in the crystal lattice. Both enantiomers had been demonstrated to intercalate into calf thymus DNA,[20] but in this study no crystals were obtained with the Δ enantiomer.

Of these binding modes, only the GG/CC step binding has any similarity with binding modes seen by us for dppz, and that is at a different step of the duplex, but we can now make a careful comparison. We have also found that the Λ-enantiomer of the phi complex causes larger increases in DNA melting temperatures, and have compared the data with that for the dppz complex. In that case the Δ-enantiomer is consistently the more stabilising Our choice of the phi ligand for this crystallographic study was based on its previous successful use for sequence recognition by the tailored rhodium complex Δ-[Rh(Me$_2$trien)phi]$^{3+}$.[21] In that case, the sequence recognition, of a GC/GC step, was driven by hydrogen bond formation between the Me$_2$trien ligands and the N7 atoms of the guanine bases, in the major groove, and was specific for the Δ-enantiomer.

Results and Discussion

To obtain crystals suitable for a diffraction experiment, 12 different oligonucleotides were selected for initial screening, and trialled using both the pure enantiomers and the racemate, as dichloride salts, giving 36 combinations. The sequences were selected to give a range of binding sites, and each trial used 96 different crystallisation conditions. Each crystallisation plate was set up in triplicate, using three different crystallisation temperatures. Thus altogether, 10,368 combinations were tested. The full list of sequences used in these trials is included as Table S4. Red crystals

were obtained after a few days from crystal screening with the d(CCGGTACCGG) sequence. These could be reproducibly obtained under a variety of conditions, using either the racemic complex or the Λ-enantiomer of [Ru(phen)$_2$phi]$^{2+}$ with the d(CCGGTACCGG) sequence. The crystallisation conditions contained Sr^{2+}, which we have already shown binds in the minor grooves at well-defined sites in the native d(TCGGTACCGA)$_4$ X-stacked Holliday junction structure. Closely related sequences, and the pure Δ-enantiomer, gave no crystals. We obtained the crystallographic unit cell with in-house equipment, and complete datasets at three wavelengths on beamline I03 at Diamond Light Source. The structure was built into a map derived by the xia2 processing package, and revealed that the central TA/TA step contained one Ru complex bound symmetrically (coinciding with a twofold axis in space group P422) and a second complex in the minor groove at the adjacent GG/CC steps. A strong anomalous signal in the Sr K edge dataset identified the cations between the duplexes as Sr^{2+}, and the map improvement permitted by using this dataset permitted the reconstruction of the remaining part of the structure. In the final model, a third Ru complex sits on a different twofold axis in space group P422, in this case with the two phen ligands stacked on cytosine bases (C2) and in effect linking the duplexes. This is an unusual space group, and generates a large solvent channel, accounting for the relatively low diffracting power of the crystals.

Space group P422 imposes strict symmetry requirements, with several components of the structure lying on special positions at 0.5 occupancy. The crystal structure of the cation had not been previously reported, so was determined in house, and the refined structure used as the starting model, with appropriate restraints, for the cation in the crystal. As shown in Figure 1b, the cation does not have an exact twofold axis, as the phi ligand shows a 6.4° curvature in the small molecule structure. We note that this curvature is modified by intercalation, discussed below. The refined structure of the complete assembly therefore requires a small amount of disorder about the twofold axes, even though the Ru atom can lie on the correct symmetry element. For Ru1, bound at the centre step, the phi ligand was aligned with the twofold symmetry, and therefore the thymine and adenine bases, giving two phen positions. For Ru3, at the terminal step, the disorder is better modelled as two phi moiety sites, so that in each case, it is the stacking with the nucleic acid component which is consistent with the required symmetry. Several details of the final refined geometries of the bound cations are discussed further below. A packing diagram and more detailed analytics are included with the Supporting Information.

Figure 1c shows the complete assembly and numbering scheme for a single duplex. The helix is unwound by the minor groove intercalation at the GG/CC steps, and at the end step the C1 and G10 residues are completely flipped out. The C1 residue is folded back into the minor groove of a symmetry related duplex, where the cytosine base stacks onto one of the phen rings of Ru2. The guanine base G10 is stacked onto a symmetry related G10, forming a guanine-rich environment for Ru3, but without direct stacking. The
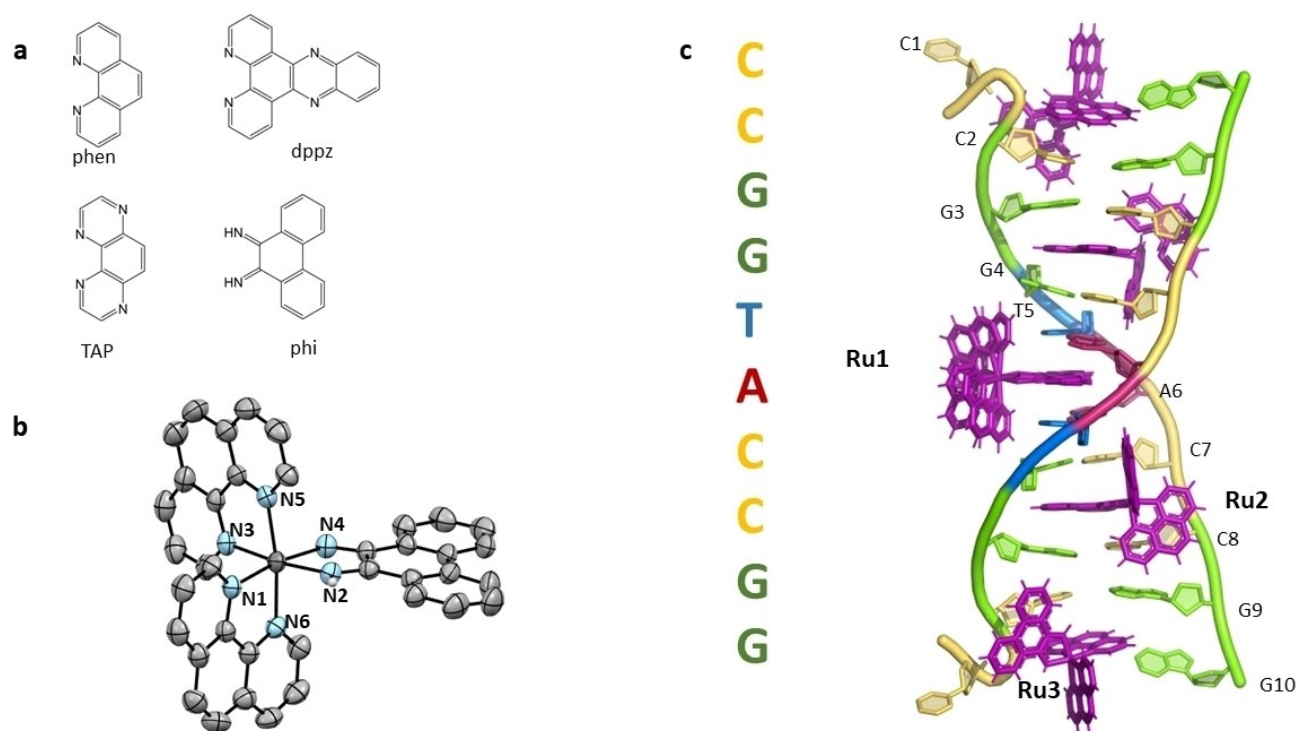
Figure 1. The completed X-ray structure. a) Ligands compared in the manuscript; b) Crystal structure of the Λ-[Ru(phen)$_2$phi]$^{2+}$ cation; c) the DNA sequence used in the X-ray work, with the colour code used throughout to conform to that of the Nucleic Acid Knowledge Base (NAKB), with the completed structure assembly. The numbering scheme corresponds to that used in the main text. Ru1 and Ru3 lie on crystallographic twofold axes, so are included in the refinement at a fixed 0.5 occupancy, even though the crystal structure of the complex, used to generate the restraints for refinement, does not have exact twofold symmetry (see discussion in the text).

overall assembly is held together by Ru3, generating a packing containing a large solvent space and some residual non-crystallographic symmetry, as revealed by the data statistics. The assembly in space group P422 contains no translational symmetry elements, but is strongly chiral, with an overall right handed suprahelical twist.

At the central TA/TA step, the phi ligand of Ru1 can be seen from Figure 2a–c to be well aligned with the thymine-adenine base pairs, with a twist angle at this symmetrical step of 33°. The phen ligands make contact with the 5-methyl group of the thymine bases, which based on some of our previous structures, may be an attractive hydrophobic interaction, and determinant of the twist angle, as discussed below. The phen ligands make no other crystal contacts.

At the GG/CC steps, there is an asymmetric cavity, reminiscent of some in our previous work,[22,23] with the unexpected feature of a hydrogen bond between the ribose oxygen of cytosine C8 and one of the NH imine groups (Figure 2d–f). To our knowledge such hydrogen bonding has not previously been seen, but would account for the preference for the angled minor groove orientation. The formation of this bond appears to generate non-planarity in the G3–C8 base pair. There is a low twist angle of 22° at this step, with close alignment of the base pairs to the phi ligand, shown in Figure 2e. This feature can contribute to a high binding constant. The stacking interactions are also shown in Figure 2e. As there are two symmetry equivalent steps per duplex, the net effect is an unwinding of the duplex by

~28°. [Ru(phen)$_2$phi]$^{2+}$ shows no photoactivity, but the rhodium analogue [Rh(phen)$_2$phi]$^{3+}$ was studied many years ago as a photocleavage agent for duplex DNA.[24] These workers reported a cleavage selectivity for the sequence 5′-CCAG-3′, where C is the cleavage position. Placed in the context of this structure, that result suggests a correspondence to the hydrogen bonded C8 of Figure 2f, and a similar binding mode and hydrogen bond formation with the triply charged Rh analogue, bringing C8 in close proximity to the photoactivated Rh centre. They also report that Rh-(phi)$_2$bpy]$^{3+}$ shows little site selectivity in its cleavage pattern. These authors suggest that the sugar could be the site of the photocleavage reaction. This unexpected structural feature, which may be confined to GG/CC steps, but would need further work, goes some way to accounting for these observations.

The environment of Ru3 is illustrated in Figure 3. The interactions at this step are essential for the formation of the crystal lattice, and show, in this case, the role of the phen ligands. With [Ru(phen)$_2$dppz]$^{2+}$ and related complexes, which always intercalate from the minor groove of a DNA duplex, depending on the sequence, the phen ligand is either positioned in the minor groove, or linking adjacent duplexes by kinking (semi-intercalation).[8,11,19] This structure shows a feature not previously observed. The two symmetry equivalent phen ligands of a single complex here link two duplexes, with each phen ligand stacked on the C2–G9 base pair and the C1 and G10 flipped out. The phi ligand is
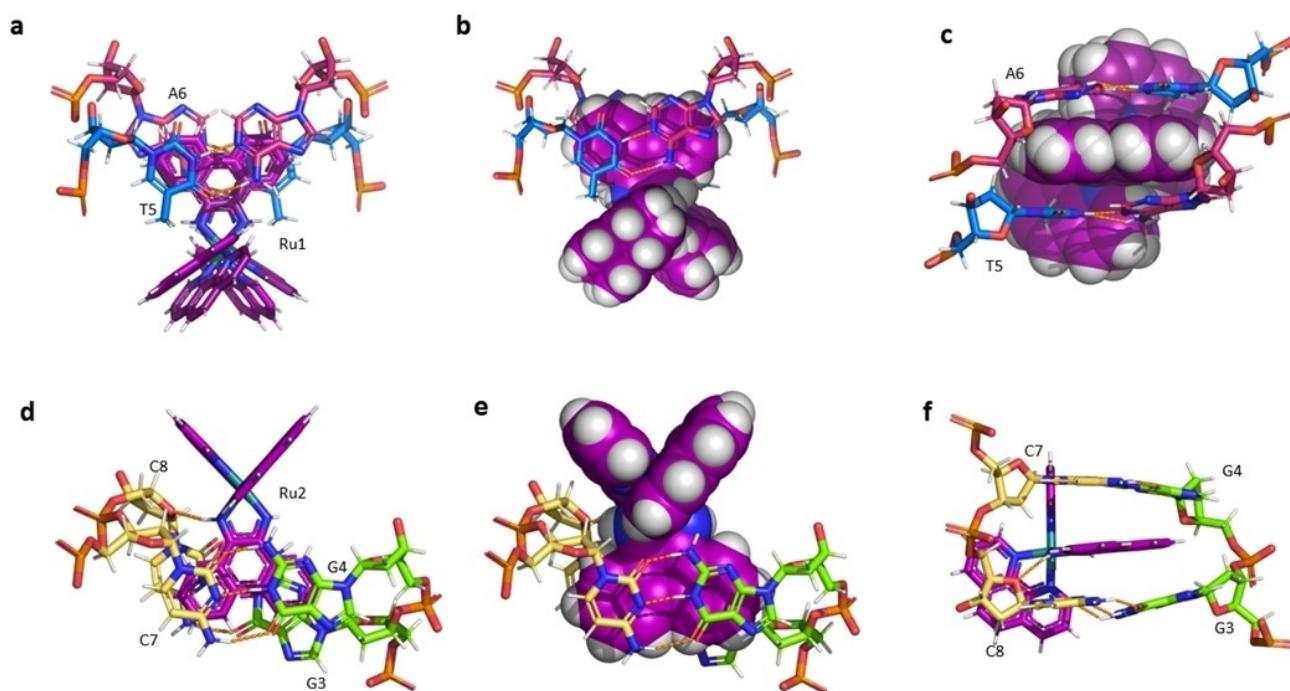
Figure 2. Major and minor groove binding. a) Ru1 in the major groove at the T5-A6 central step of the duplex. This site lies on a twofold axis, and the bending of the phi ligand results in disorder of the phen ligands. The TA/TA twist angle is 33°; b) the same view in spacefill to show the excellent match of the base pairs to the phi moiety; c) the model in b) rotated to show the intercalation cavity from the minor groove side d) Ru2 showing angled intercalation and hydrogen bond formation at the G3—G4/C7—C8 step. The hydrogen bond is between O4' of C8 and the near imine N—H. (O—N distance 3.1 Å). The projection is from the C7—G4 base pair side. The G3—G4/C7—C8 step shows angled intercalation and a low twist angle of 22°; e) the same view with the complex as spacefill to show the almost parallel stacking of the base pair and the phi moiety; f) stick view into the major groove, showing the C8-imine H bond formation and the apparent disruptive effect of this H bond formation on the C8—G3 base pair.
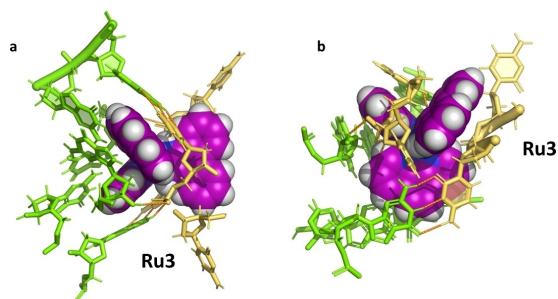

Figure 3. Linking of the duplexes by Ru3. a) View showing the twofold symmetry of the site; b) view showing the stacking interaction between the phen ligand and the C2—G9 base pair. The flipped out C1 stacks onto a phen moiety of Ru2 (not shown for clarity).

unbound. The phen ligand is not known for parallel intercalation, but rather, for kinking from the minor groove, and, in contrast, this is an example where it is oriented parallel to a base pair. The overall result is an approximately orthogonal orientation of the two intersecting duplexes.

In complementary solution work, we first made some DNA melting temperature comparisons. The structure presented here is a striking contrast to the body of structural evidence on binding modes of the ruthenium complex [Ru(phen)$_2$dppz]$^{2+}$.[19,25] In both cases, the Λ-enantiomer was

strongly preferred in crystallisation experiments with the d(CCGGTACCGG) sequence, and it is difficult to explore the step preferences of either complex in a systematic way using crystallographic methods. As stated in the Introduction, for the self-complementary decamers of sequence d(CCN1N2N3n3n2n1GG), a rare example of a systematic study examined the formation of A-DNA, B-DNA or junction DNA by all 64 combinations of N1N2N3.[3] The sequence d(CCGGTACCGG) was the only one to consistently form junctions as the native, and was subsequently shown to bind a bis-acridine ligand.[9,10] Because of the invariable crystallisation in junction form, the sequence can also form a mixture of species in solution, which could complicate a melting temperature study.[4] As we have seen with both the dppz and the phi complexes, metal complex binding stabilises the B-DNA form by intercalation. We therefore compared all ten permutations which can be made from the d(CCGGN1N2CCGG) decamers. For each, we determined the melting temperature of both enantiomers of [Ru(phen)$_2$phi]$^{2+}$ and both enantiomers of [Ru-(phen)$_2$dppz]$^{2+}$. These experimental conditions therefore differ only at the centre step of the decamer duplex and the intercalating ligand. The results are summarised in Figure 4 and tabulated in full in Table S6. The x-axis of the plot uses the stacking energies of the ten steps derived by Frank-Kamenetskii and co-workers.[12] Most obviously, both Λ-
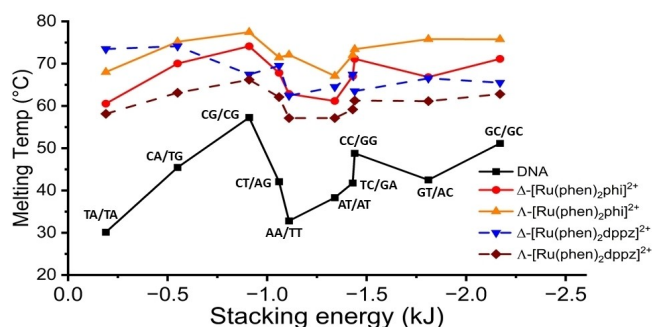
GDCh

Research Articles

Angewandte
Chemie
International Edition

Figure 4. Comparison of melting temperature increases. In ten decamer sequences d(CCGGN1 N2CCGG) - both enantiomers of [Ru-(phen)$_2$dppz]$^{2+}$ and of [Ru(phen)$_2$phi]$^{2+}$ were measured with all ten permutations of N1 and N2, in each case in a ratio of 1 Ru complex per duplex. The horizontal axis uses the base pair stacking energies from ref [12].

enantiomers show the same pattern, with the phi complex consistently higher by ~10 °C. The Λ-phi complex is also consistently higher than the Δ-enantiomer. The converse is true for the two dppz enantiomers, and here the Δ-enantiomer is consistently more stabilising. These conclusions are valid wherever in the duplex each complex binds.[26] Using natural and polymeric DNAs, as previously reported, both enantiomers have high binding constants, but can be distinguished by luminescence and other criteria.[27]

We then examined the solution behaviour[28] of the [Ru(phen)$_2$phi]$^{2+}$ enantiomers with a wider range of natural and synthetic DNAs, in a series of direct and indirect experiments (Figure 5). Firstly, electronic absorption spectroscopy was employed using calf-thymus DNA (ctDNA) to calculate the intrinsic binding constants K_b. To quantitatively compare the binding affinity of each enantiomer to ctDNA, K_b values were calculated using the following equation:

$$[DNA]/(\varepsilon_a-\varepsilon_f) = [DNA/(\varepsilon_b-\varepsilon_f) + 1/K_b(\varepsilon_b-\varepsilon_f)) \quad (1)$$

where: ε_a = apparent complex extinction coefficient, ε_f = free complex extinction coefficient and, ε_b = bound complex extinction coefficient. By plotting $[DNA]/(\varepsilon_a-\varepsilon_f)$ versus [DNA], K_b values were calculated from the ratio of the slope to the intercept; slope = $1/(\varepsilon_b-\varepsilon_f)$ and intercept = $1/K_b(\varepsilon_b-\varepsilon_f)$. The K_b values obtained for Λ-[Ru(phen)$_2$phi]$^{2+}$ and Δ-[Ru(phen)$_2$phi]$^{2+}$ were 46.23×10^3 M^{-1} and 47.12×10^3 M^{-1} respectively (Figure 5a). These results suggest that both enantiomers bind long DNA polymers with similar affinity and are in good agreement with the earlier K_b value reported for the racemic [Ru(phen)$_2$phi]$^{2+}$ (46.8×10^3 M^{-1}).[29] Next, the inhibition of supercoiled plasmid DNA (pUC19) unwinding by topoisomerase I (Topo-I) was examined in the presence of both enantiomers. This assay allows for identification of intercalation which, in turn, inhibits Topo-I from mediating the relaxation of negatively supercoiled (SC) pUC19 (Figure 5b, lanes 1 and 15).[30] Upon titration with increasing concentrations of Λ-[Ru(phen)$_2$phi]$^{2+}$ and Δ-[Ru-(phen)$_2$phi]$^{2+}$ (Figure 5b, lanes 3–14 and 17–28) the profile

changes remarkably with both Ru(II) complexes intercalatively converting negatively supercoiled pUC19 (−) to the positive (+) form, which is not recognised by the Topo-I enzyme.

To probe the sequence-specific binding preferences of the enantiomers, a series of hairpin dodecamers with varying AT and GC sequence content were designed. These hairpin sequences contain short adenine loops and a 5′-Alexa Fluor 647 (F) modification suitable for direct analysis through microscale thermophoresis (MST), a relatively new technique that enables direct binding (K_d) analysis, based on thermophoretic changes induced within a target biomolecule in the presence of a bound drug (Figure 5c).[31]

Comparison between both enantiomers reveals enhanced intercalation by Λ-[Ru(phen)$_2$phi]$^{2+}$ due to the earlier onset of positively supercoiled pUC19 (0.7 μM) compared to the Δ-[Ru(phen)$_2$phi]$^{2+}$ enantiomer (0.9 μM).

Here, binding of Λ-[Ru(phen)$_2$phi]$^{2+}$ to the Dickerson–Drew hairpin sequence (F-DDH) displayed a K_d value of 580 nM, while for the Δ-[Ru(phen)$_2$phi]$^{2+}$ enantiomer a lower affinity K_d value of 1 μM was obtained. Furthermore, in the GC rich F–D7H hairpin sequence, the K$_d$ values were similar to those obtained for the F-DDH sequence. Next, a TATA-rich hairpin sequence (D6AH) was tested and here both enantiomers displayed significant binding interactions with K_d values of 520 nM and 600 nM calculated for Λ-[Ru(phen)$_2$phi]$^{2+}$ and Δ-[Ru(phen)$_2$phi]$^{2+}$ enantiomers respectively. Finally, the results obtained for the GGCC-rich hairpin sequence (F-TP), revealed the Λ-[Ru(phen)$_2$phi]$^{2+}$ enantiomer to have a greater affinity K_d value (430 nM) compared to the Δ-[Ru(phen)$_2$phi]$^{2+}$ enantiomer (960 nM). Overall, it is clear that the Λ-enantiomer has significantly higher binding properties towards these palindromic sequences compared to the Δ-enantiomer. In every case the Λ-enantiomer showed higher affinity and it is notable that in three of the four sequences examined, the K_d value was almost half of that obtained for the Δ-enantiomer. Following MST analysis, FRET melting experiments with sequences FRET-D7H, -D6AH, and -DTP in the presence of increasing concentrations of both enantiomers were performed (Figure 5d). These sequences match those examined by MST analysis but in addition to the presence of a 5′-Alexa Fluor 647 (F) modification, also contain a 3′-Iowa Black RQ quencher. In all experiments, the Λ-[Ru(phen)$_2$phi]$^{2+}$ enantiomer exhibited greater thermal stabilisation, with melting curves reaching a plateau at significantly lower concentrations compared to the Δ-[Ru(phen)$_2$phi]$^{2+}$ enantiomer. Differences were particularly notable within the TATA rich sequence, FRET-D6AH, where the melting profiles of the enantiomers diverge significantly, again showing a strong Λ preference. This divergence was not prominent in the MST analysis of F-D6AH (where K_d values of 520 nM and 600 nM were identified for the Λ- and Δ-enantiomers, respectively). This result is consistent with the different principle of MST. It measures total affinity based on the overall binding of the complex—combining electrostatic, groove binding, and intercalation interactions—which result in changes to the hydration shell, shape, and charge of the DNA duplex. However, for the FRET thermal melting

Angew. Chem. Int. Ed. **2024**, e202318863 (5 of 10) © 2024 The Authors. Angewandte Chemie International Edition published by Wiley-VCH GmbH

15213773, 0, Downloaded from https://onlinelibrary.wiley.com/doi/10.1002/anie.202318863 by Test, Wiley Online Library on [29/02/2024]. See the Terms and Conditions (https://onlinelibrary.wiley.com/terms-and-conditions) on Wiley Online Library for rules of use; OA articles are governed by the applicable Creative Commons License

Figure 5. Binding analyses. a) Direct UV/Vis DNA binding analysis of Λ-[Ru(phen)$_2$phi]$^{2+}$ and Δ-[Ru(phen)$_2$phi]$^{2+}$ complexes with titrated ctDNA plotted as [DNA]/($\varepsilon_a-\varepsilon_f$) versus [DNA]; b) Topoisomerase I-mediated relaxation assay with pUC19 (400 ng) in the presence of increasing concentrations (0.1–2.0 μM) of Λ-[Ru(phen)$_2$phi]$^{2+}$ and Δ-[Ru(phen)$_2$phi]$^{2+}$; c) Binding isotherms of Λ-[Ru(phen)$_2$phi]$^{2+}$ and Δ-[Ru(phen)$_2$phi]$^{2+}$ complexes with hairpin sequences obtained via microscale thermophoresis (MST); d) FRET thermal melting analysis of Λ-[Ru(phen)$_2$phi]$^{2+}$ and Δ-[Ru(phen)$_2$phi]$^{2+}$ complexes with palindromic hairpin sequences. Analysis was performed on a Roche LightCycler 480 II using multiple *r* values per experiment.

experiments examined here, the greatest contribution to denaturation is likely to be intercalation, and it is this difference that is identifiable during FRET analysis.

To corroborate the binding interactions of both enantiomers with specific palindromic sequences, UV thermal melting analysis was performed using a series of dodecamers in the presence of both complexes at an *r* value of 0.5

(Table 1).[28] Sequence D1, identical in composition to D7H, was moderately stabilised by both Λ-[Ru(phen)$_2$phi]$^{2+}$ (+ 7.6°C) and Δ-[Ru(phen)$_2$phi]$^{2+}$ (+4.3°C) enantiomers. This stability was enhanced slightly in sequence D2, where cytosine (C) bases were replaced with 5-meth-yldeoxycytosine (5 mC). The binding mode here is likely to be at the CC/GG step, corresponding to the angled minor

Table 1: UV thermal melting properties. Palindromic dodecamers in the presence of Δ- and Λ-[Ru(phen)$_2$(phi)]$^{2+}$ enantiomers at an r loading of 0.5 (where r=[Ru]/[DNA]), or 1 Ru complex per DNA duplex.

Duplex		D1	D2	D3	D4	D5	D6	Duplex	Sequence
DNA (control)	T_M (°C)	68.00	74.64	72.29	67.28	49.56	47.71	D1	d(ATCGGCGCCGAT)$_2$
Λ-[Ru(phen)$_2$(phi)]$^{2+}$	T_M (°C)	75.55	85.48	78.37	75.12	71.93	73.29	D2	d(ATMGGMGMMGAT)$_2$
	ΔT_M (°C)	+7.55	+10.84	+6.08	+7.84	+22.37	+25.58	D3	d(GCCGGTACCGGC)$_2$
Δ-[Ru(phen)$_2$(phi)]$^{2+}$	T_M (°C)	72.32	79.76	74.71	71.41	55.30	51.48	D4	d(GCCGGATCCGGC)$_2$
	ΔT_M (°C)	+4.32	+5.12	+2.42	+4.13	+5.74	+3.77	D5	d(GCTTTATAAAGC)$_2$
M = 5-methyl-C; U = Uracil								D6	d(GCUUUAUAAAGC)$_2$

groove binding of Ru2 in the structure reported here (Figures 2d–f). Methylation of adjacent C could lower the native duplex melting temperature by local disruption of the ordered hydration, compensated by a higher stacking energy at low twist angle (Figure 2e) and perhaps a stronger hydrogen bond (Figure 2f). For melting experiments with sequences containing central TA/TA (D3) and AT/AT (D4) steps, the Λ-enantiomer was again notably more effective than the Δ-enantiomer. Finally, a TATA-rich palindromic dodecameric sequence (D5) was examined and showed preferential binding of Λ-[Ru(phen)$_2$phi]$^{2+}$ with remarkable stabilisation (+22.4°C). Significantly, in the presence of Δ-[Ru(phen)$_2$phi]$^{2+}$, only a moderate ΔT_m value was obtained (+5.8°C). To probe this finding further, sequence D6 was tested in which thymine (T) was substituted with uracil (U). In this case, removal of the methyl groups on opposing strands produced a small further stabilisation. The binding mode here is likely to be that shown for Ru1 in Figures 2a–c, symmetrical intercalation from the major groove at a TA/TA step. A high twist angle, as seen here, brings the 5-Me positions on opposing strands closer together in the major groove, and the absence of these groups in uracil, could allow a better stacking overlap. The main result from these assays which cannot be interpreted in terms of the binding modes seen in this work is the remarkable stabilisation of the TATA sequence by the Λ-enantiomer. Unexpectedly, this is a much bigger effect than that of changing the methylation state of pyrimidines (see discussion below).

In 2012, it was shown by X-ray crystallography that the Δ-enantiomer of [Ru(phen)$_2$dppz]$^{2+}$ bound in the minor groove of the d(CGGAAATTACCG)$_2$ duplex, with binding by insertion (flipping out) at the AA mismatched step.[32] Both enantiomers of [Ru(phen)$_2$dppz]$^{2+}$ were found to intercalate from the minor groove of the hexamer duplex d(ATCGAT)$_2$.[22] The persistence of these binding distinctions in solution was shown using ultrafast laser spectroscopy and the photooxidising [Ru(TAP)$_2$dppz]$^{2+}$ complex (TAP=tetraazaphenanthrene).[26] An extended dppz skeleton was recently used to show that a specific G-quadruplex, the antiparallel chair topology of the human telomeric DNA sequence, could be stabilised by Λ-[Ru(phen)$_2$qdppz]$^{2+}$, where qdppz is an extended bent ligand containing an anthraquinone moiety.[33] In that case, there is strong and oriented stacking on the G-quartet surface, sandwiched by a TTA loop to give a binding mode which is also primarily stabilised by stacking and other hydrophobic interactions. The binding mode can be directly paralleled by the powerful

suppression of DNA replication in a template DNA strand containing the same sequence. These binding modes can now be said to be well understood, with the crystallographic results complemented by a range of solution studies. In recent years, the cellular take up of Ru-dppz compounds has been of considerable interest because of the therapeutic and diagnostic (combined as theranostic) capability. In that context, recent papers show great progress, encompassing diruthenium compounds, compounds for photodynamic therapy, and the use of counteranions to facilitate cellular takeup.[34–39]

In contrast, studies of DNA binding by the diimine complex [Ru(phen)$_2$phi]$^{2+}$ have a longer history than that of the dppz complexes, dating back to the 1980s, but with binding modes much less well understood. This complex was first synthesised as part of the early work on mixed ligand complexes of ruthenium binding to DNA.[29] The dimensions of the phi ligand match those of a DNA base pair, and high binding constants with calf thymus DNA were recorded,[29] but attention switched to the Rh(III) analogue, [Rh-(phen)$_2$phi]$^{3+}$, as it had efficient DNA photocleavage properties which could be developed further.[24] A nonplanar extended phi ligand (chrysi) was subsequently used for mismatch recognition, binding by insertion from the minor groove.[40,41]

We can then ask—how do dppz and phi compare as intercalating ligands? Our extensive crystallographic studies of [Ru(phen)$_2$dppz]$^{2+}$ cations with a range of duplex and quadruplex forming DNA sequences have shown that, for duplexes, the direction of intercalation is from the minor groove and that, unless at a TA/TA system the orientation within the groove is angled, making contact to at least one component of the intercalation cavity (Figure 6). Most typically, this interaction is with the sugar component of the backbone. With quadruplexes, the typical mode is stacking at a terminal G-quartet with the Ru(phen)$_2$ moiety in a wide groove between antiparallel strands. We can now say with some confidence that at a TA/TA step, the major groove binding mode seen here is the counterpart to that with dppz, symmetrical intercalation, but from opposite grooves, by the Λ-enantiomer. As shown in Figure 7, the phi chromophore is parallel to the long axis of the TA/TA base pairs, with a twist angle of 33° whereas the dppz chromophore is orthogonal, and accompanied by a twist angle close to 40°. At the GG/CC step, both moieties are angled (canted) in the minor groove, but again with a lower twist of 22° for the phi ligand compared with 26° for the dppz ligand. Thus in
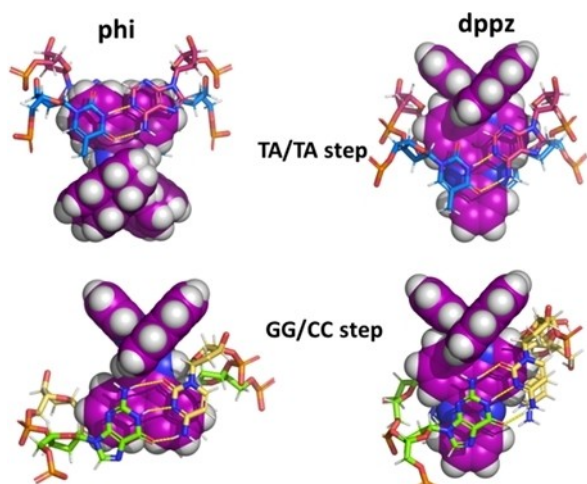
Figure 6. Comparison with dppz binding modes. Comparison of the two intercalated phi ligands in this structure with those previously observed for dppz intercalation. The minor groove is on the upper side in each case.
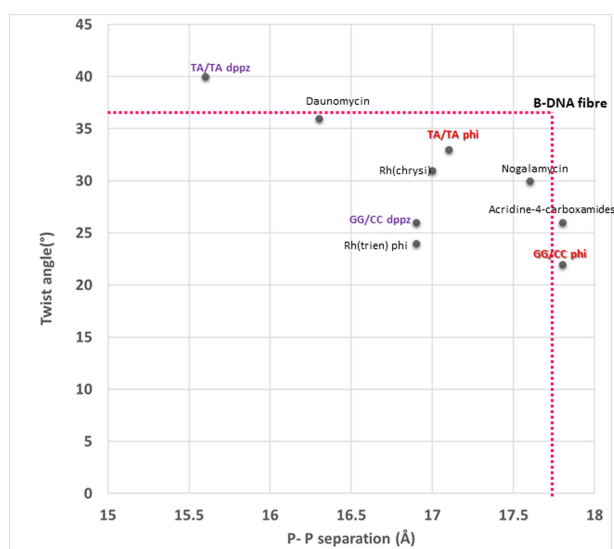

Figure 7. Twist angles vs P–P separations compared with classic B-DNA fibre parameters. PDB codes used to derive the data as follows:— Dppz—3U38; Daunomycin 1VTH; Rh-chrysi 2O1I; Rh(trien)phi 454D; Nogalamycin 182D; acridine-4-carboxamide 367D.

each case, the phi ligand causes greater unwinding of the DNA helix. Another way of representing the differences is shown in the graph of Figure 7. Here, the twist angles of several intercalation cavities for which accurate structural details are available are plotted against the P–P separation across the intercalation cavity. Compared with the classic B-DNA fibre parameters, intercalation mainly results in a closer P–P separation. There is a clear trend, with a high twist angle, most obviously that seen for dppz at the TA/TA step associated with a small P–P separation. This is not surprising, as the high twist is connected to the stacking of the phen ligands on the ribose sugars. At the other extreme, the low twist of the phi ligand at the GG/CC steps is

accompanied by a larger P–P separation, in a way previously seen in several acridine-4-carboxamide structures, and again where the long axis of the ligand is approximately parallel to the long axes of the cavity base pairs.

A structural comparison of the flexibility of phi and dppz as ligands is now also possible. What we have noted in this work is the susceptibility of the phi ligand to geometrical changes which depend on the local environment. The refinement of the structure was carried out using the program phenix-refine. For the ruthenium complex, as we have seen, there are three different environments in the crystal. Starting from the coordinates of the [Ru-(phen)$_2$phi]$^{2+}$ cation, the crystallographic restraints allow limited movement of the atomic positions. Unlike the dppz ligand, the phi ligand forms Ru–N bonds which are shorter than the Ru–N bonds formed with phen, indicating some multiple bond character. The bound ions all show a further degree of shortening of the Ru–N(imine) bonds, as shown in Figure S5. The exception is the bond in Ru2 to the hydrogen bonded imine N, which is lengthened rather than shortened. The average distance is 2.02 Å in the unbound complex, shortening to 1.98 Å in the bound complex, but, unexpectedly, 2.04 Å for the hydrogen bonded imine. Perhaps this bond lengthening can be linked to increasing reactivity at that site. The DNA photodamaging properties of the rhodium analogue [Rh(phen)$_2$phi]$^{3+}$ were reported many years ago by Pyle.[24,42] Also notable is the variation in the bend of the phi ligand in the three different sites. for Ru1 it is increased to 12.0°, but for Ru2 it is decreased to 4.2°. For Ru3, in which the phi ligand does not make stacking interactions, the angle remains at 6.9°. These structural effects of intercalation are more marked than those seen with the rather inflexible dppz, but have a parallel in the 12° bend induced in the anthraquinone moiety of the extended qdppz ligand on binding to the nonplanar G-quartet surface in the antiparallel chair topology, recently reported by us.[33]

A final structural comment relates to groove geometries. In previous studies we have analysed extensively the effect that the residues adjacent to an intercalation site have on the orientation of the intercalated species when compared to the long axis of the DNA base pairs.[43–45] In the minor groove, the principal steric constraint is the 2-NH$_2$ substituent on an adjacent guanine, which has the effect of favouring an angled orientation of the dppz ligand, and a symmetrical, perpendicular intercalation mode has never been observed in that case.[23] In the major groove the main distinguishing steric feature is the presence or absence of the 5-methyl substituent.[46] In the standard base pairing, therefore, the AT basepair is more sterically hindered in the major groove. Figure 8 shows two scenarios relevant to the dodecamer comparisons made in this study. Figure 8a shows a low twist angle at an intercalation cavity formed at a TT/AA step, comparable to the Ru2 environment seen in this work, which is the case where intercalation causes unwinding of the helix. Here, with the methyl groups on the same strand, intercalation may be more stabilising when methyl groups are present. Figure 8b shows a high twist angle at a TA/TA step, as seen in the environment of Ru1 in this work. In that case, the high twist angle increases the winding of the helix,
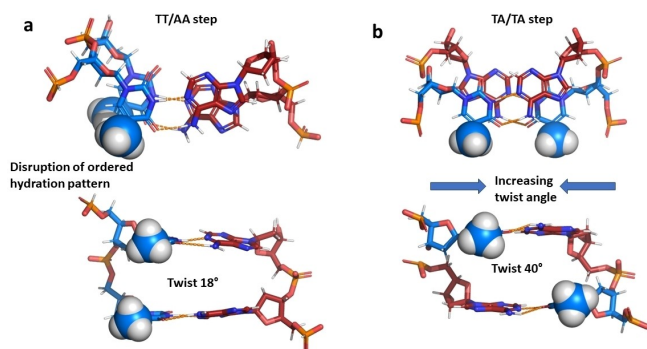
Angew. Chem. Int. Ed. **2024**, e202318863 (8 of 10)

© 2024 The Authors. Angewandte Chemie International Edition published by Wiley-VCH GmbH

Figure 8. Pyrimidine methylation. a) low twist angle with adjacent pyrimidine methylation (TT/AA step); b) high twist angle with opposing pyrimidine methylation (TA/TA step). Each step shown in two views.

bringing the opposing methyl groups closer. Here, in contrast, intercalation may be more stabilising in the absence of methyl group.

Finally, the overall solution finding is that, whatever the DNA sequence, the melting temperature data and ethidium displacement data show that the Λ-enantiomer is consistently more stabilising. Particularly notable is the $<20°$ stabilisation of the d(GCTTTATAAAGC) and d-(GCUUUAUAAAGC) duplex sequences, which include the TATA box promotor consensus sequence.[47,48] As shown in Figure 8, the structural difference between these two duplexes is the presence or absence of the 5-methyl group in the major groove. The absence of the methyl group makes a small difference, which would be consistent with the symmetrical major groove binding mode seen in this work, but does not account for the striking effect of the presence of the two adjacent TA/TA steps on the big enhancement of the Λ-preference, starting from the low melting temperatures of these native sequences. It is possible that this sequence permits a different binding mode such as semi-intercalation (kinking) or insertion, or a combination of these, which would be highly stabilising.[32,49]

Conclusion

This work provides the first structural evidence that it is possible for a ruthenium polypyridyl complex to intercalate from the major groove of a B-DNA duplex, making use of a diimine ligand, phi. Unexpectedly, the binding modes of this Λ-complex are sequence selective, with symmetrical major groove binding at the central TA/TA step, and canted minor groove binding at the GG/CC steps of the palindromic sequence. As a consequence, this cation can be considered a useful building block in the development of more elaborate constructs designed to recognise sequence specific features in the DNA major groove, such as those obtained with triplex forming oligonucleotides.[15,18,28,31,50] In contrast, ruthenium complexes with the dppz intercalating ligand always intercalate from the minor groove. These conclusions are reinforced by solution data showing that the Λ-enantiomer is always more stabilising in a range of systems, as shown by

DNA melting temperature, and a strong preference for the TATA sequence, whereas for the dppz-type complexes, the Δ-enantiomer is consistently more stabilising. Furthermore, differential behaviour is also seen in topoisomerase I inhibition assays and ethidium bromide displacement assays. The Λ-[Ru(phen)₂phi]²⁺ cation is now seen to be a useful building block for the construction of major groove specific binding assemblies.

Conflict of Interest

The authors declare no conflict of interest.

Data Availability Statement

The data that support the findings of this study are openly available in wwPDB (Protein Data Bank) at https://www.https://www.wwpdb.org/pdb?id=pdb_00008oyr, reference number 1292130302.

[1] M. Ortiz-Lombardía, A. González, R. Eritja, J. Aymamí, F. Azorín, M. Coll, *Nat. Struct. Biol.* **1999**, *6*, 913–917.

[2] D. M. J. Lilley, *Proc. Nat. Acad. Sci.* **2002**, *94*, 9513–9515.

[3] F. A. Hays, A. Teegarden, Z. J. R. Jones, M. Harms, D. Raup, J. Watson, E. Cavaliere, P. S. Ho, *Proc. Natl. Acad. Sci. USA* **2005**, *102*, 7157–62.

[4] F. A. Hays, V. Schirf, P. S. Ho, B. Demeler, *Biochemistry* **2006**, *45*, 2467–2471.

[5] J. H. Thorpe, B. C. Gale, S. C. M. Teixeira, C. J. Cardin, *J. Mol. Biol.* **2003**, *327*, 97–109.

[6] C. J. Cardin, J. H. Thorpe, B. C. Gale, S. C. M. Teixeira, "Strontium, a MAD target for the DNA Holliday junction," DOI 10.2210/PDB1NVY/PDBcan be found under http://www.rcsb.org/structure/1NVY.

[7] A. Naseer, C. J. Cardin, "Strontium bound to the Holliday junction sequence d(TCGGCGCCGA)4," DOI 10.2210/PDB3GOO/PDBcan be found under https://www.rcsb.org/structure/3GOO.

[8] J. P. Hall, K. O'Sullivan, A. Naseer, J. A. Smith, J. M. Kelly, C. J. Cardin, *Proc. Nat. Acad. Sci.* **2011**, *108*, 17610–17614.

Angew. Chem. Int. Ed. **2024**, e202318863 (9 of 10)

© 2024 The Authors. Angewandte Chemie International Edition published by Wiley-VCH GmbH

[9] A. L. Brogden, N. H. Hopcroft, M. Searcey, C. J. Cardin, *Angew. Chem. Int. Ed.* **2007**, *46*, 3850–3854.

[10] K. T. McQuaid, A. Pipier, C. J. Cardin, D. Monchaud, *Nucleic Acids Res.* **2022**, *50*, 12636–12656.

[11] H. Niyazi, J. P. Hall, K. O'Sullivan, G. Winter, T. Sorensen, J. M. Kelly, C. J. Cardin, *Nat. Chem.* **2012**, *4*, 621–628.

[12] E. Protozanova, P. Yakovchuk, M. D. Frank-Kamenetskii, *J. Mol. Biol.* **2004**, *342*, 775–785.

[13] G. Wang, M. M. Seidman, P. M. Glazer, *Science* **1996**, *271*, 802–805.

[14] P. A. Havre, E. J. Gunther, F. P. Gasparro, P. M. Glazer, *Proc. Nat. Acad. Sci.* **1993**, *90*, 7879–7883.

[15] N. Z. Fantoni, T. Brown, A. Kellett, *ChemBioChem* **2021**, *22*, 2184–2205.

[16] B. McGorman, N. Z. Fantoni, S. O'Carroll, A. Ziemele, A. H. El-Sagheer, T. Brown, A. Kellett, *Nucleic Acids Res.* **2022**, *50*, 5467–5481.

[17] M. Flamme, E. Clarke, G. Gasser, M. Hollenstein, *Molecules* **2018**, *23*, 28–31.

[18] T. Lauria, C. Slator, V. McKee, M. Müller, S. Stazzoni, A. L. Crisp, T. Carell, A. Kellett, *Chem. Eur. J.* **2020**, *26*, 16782–16792.

[19] C. J. Cardin, J. M. Kelly, S. J. Quinn, *Chem. Sci.* **2017**, *8*, 4705–4723.

[20] K. Naing, M. Takahashi, M. Taniguchi, A. Yamagishi, *Bull. Chem. Soc. Jpn.* **1997**, *67*, 2424–2429.

[21] C. L. Kielkopf, K. E. Erkkila, B. P. Hudson, J. K. Barton, D. C. Rees, *Nat. Struct. Biol.* **2000**, *7*, 117–121.

[22] J. P. Hall, D. Cook, S. R. Morte, P. McIntyre, K. Buchner, H. Beer, D. J. Cardin, J. A. Brazier, G. Winter, J. M. Kelly, C. J. Cardin, *J. Am. Chem. Soc.* **2013**, *135*, 12652–12659.

[23] J. P. Hall, S. P. Gurung, J. Henle, P. Poidl, J. Andersson, P. Lincoln, G. Winter, T. Sorensen, D. J. Cardin, J. A. Brazier, others, *Chem. Eur. J.* **2017**, *23*, 4981–4985.

[24] A. M. Pyle, E. C. Long, J. K. Barton, *J. Am. Chem. Soc.* **1989**, *111*, 4520–4522.

[25] C. J. Cardin, K. T. McQuaid, in *Handb. Chem. Biol. Nucleic Acids* (Ed.: N. Sugimoto), Springer Nature Singapore, Singapore **2022**, pp. 1–33.

[26] P. M. Keane, F. E. Poynton, J. P. Hall, I. V. Sazanovich, M. Towrie, T. Gunnlaugsson, S. J. Quinn, C. J. Cardin, J. M. Kelly, *Angew. Chem. Int. Ed.* **2015**, *54*, 8364–8368.

[27] C. Hiort, P. Lincoln, B. Norden, *J. Am. Chem. Soc.* **1993**, *115*, 3448–3454.

[28] A. Kellett, Z. Molphy, C. Slator, V. McKee, N. P. Farrell, *Chem. Soc. Rev.* **2019**, *48*, 971–988.

[29] A. M. Pyle, J. P. Rehmann, R. Meshoyrer, C. V. Kumar, N. J. Turro, J. K. Barton, *J. Am. Chem. Soc.* **1989**, *111*, 3051–3058.

[30] C. Slator, Z. Molphy, V. McKee, C. Long, T. Brown, A. Kellett, *Nucleic Acids Res.* **2018**, *46*, 2733–2750.

[31] A. Gibney, R. E. F. de Paiva, V. Singh, R. Fox, D. Thompson, J. Hennessy, C. Slator, C. J. McKenzie, P. Johansson, V. McKee, F. Westerlund, A. Kellett, *Angew. Chem. Int. Ed.* **2023**, *62*, e202305759.

[32] H. Song, J. T. Kaiser, J. K. Barton, *Nat. Chem.* **2012**, *4*, 615–620.

[33] K. T. McQuaid, S. Takahashi, L. Baumgaertner, D. J. Cardin, N. G. Paterson, J. P. Hall, N. Sugimoto, C. J. Cardin, *J. Am. Chem. Soc.* **2022**, *144*, 5956–5964.

[34] K. L. Smitten, H. M. Southam, J. B. de la Serna, M. R. Gill, P. J. Jarman, C. G. W. Smythe, R. K. Poole, J. A. Thomas, *ACS Nano* **2019**, *13*, 5133–5146.

[35] K. L. Smitten, S. D. Fairbanks, C. C. Robertson, J. B. de la Serna, S. J. Foster, J. A. Thomas, *Chem. Sci.* **2019**, *11*, 70–79.

[36] A. Raza, S. A. Archer, S. D. Fairbanks, K. L. Smitten, S. W. Botchway, J. A. Thomas, S. MacNeil, J. W. Haycock, *J. Am. Chem. Soc.* **2020**, *142*, 4639–4647.

[37] J. Karges, F. Heinemann, M. Jakubaszek, F. Maschietto, C. Subecz, M. Dotou, R. Vinck, O. Blacque, M. Tharaud, B. Goud, E. Viñuelas Zahínos, B. Spingler, I. Ciofini, G. Gasser, *J. Am. Chem. Soc.* **2020**, *142*, 6578–6587.

[38] R. Huang, C.-H. Huang, J. Chen, Z.-Y. Yan, M. Tang, J. Shao, K. Cai, B.-Z. Zhu, *Nucleic Acids Res.* **2023**, *51*, 11981–11998.

[39] X.-J. Chao, C.-H. Huang, M. Tang, Z.-Y. Yan, R. Huang, Y. Li, B.-Z. Zhu, *Nucleic Acids Res.* **2023**, *51*, 3041–3054.

[40] V. C. Pierre, J. T. Kaiser, J. K. Barton, *Proc. Natl. Acad. Sci. USA* **2007**, *104*, 429–434.

[41] B. M. Zeglis, V. C. Pierre, J. T. Kaiser, J. K. Barton, *Biochemistry* **2009**, *48*, 4247–4253.

[42] K. E. Erkkila, D. T. Odom, J. K. Barton, *Chem. Rev.* **1999**, *99*, 2777–2795.

[43] P. Keane, J. Hall, F. Poynton, B. Poulsen, S. Gurung, I. Clark, I. Sazanovich, M. Towrie, T. Gunnlaugsson, S. Quinn, C. Cardin, J. M. Kelly, *Chem. Eur. J.* **2017**, DOI 10.1002/chem.201701447.

[44] P. M. Keane, F. E. Poynton, J. P. Hall, I. P. Clark, I. V. Sazanovich, M. Towrie, T. Gunnlaugsson, S. J. Quinn, C. J. Cardin, J. M. Kelly, *J. Phys. Chem. Lett.* **2015**, *6*, 734–738.

[45] P. M. Keane, K. O'Sullivan, F. E. Poynton, B. C. Poulsen, I. V. Sazanovich, M. Towrie, C. J. Cardin, X.-Z. Sun, M. W. George, T. Gunnlaugsson, S. J. Quinn, J. M. Kelly, *Chem. Sci.* **2020**, *11*, 8600–8609.

[46] J. F. Kribelbauer, X.-J. Lu, R. Rohs, R. S. Mann, H. J. Bussemaker, *J. Mol. Biol.* **2020**, *432*, 1801–1815.

[47] C. Yang, E. Bolotin, T. Jiang, F. M. Sladek, E. Martinez, *Gene* **2007**, *389*, 52–65.

[48] S. K. Burley, *Curr. Opin. Struct. Biol.* **1996**, *6*, 69–75.

[49] H. Song, *Recognition of Nucleic Acid Mismatches by Luminescent Ruthenium Complexes*, PhD, California Institute of Technology **2012**.

[50] J. Hennessy, B. McGorman, Z. Molphy, N. P. Farrell, D. Singleton, T. Brown, A. Kellett, *Angew. Chem. Int. Ed.* **2022**, *61*, e202110455.
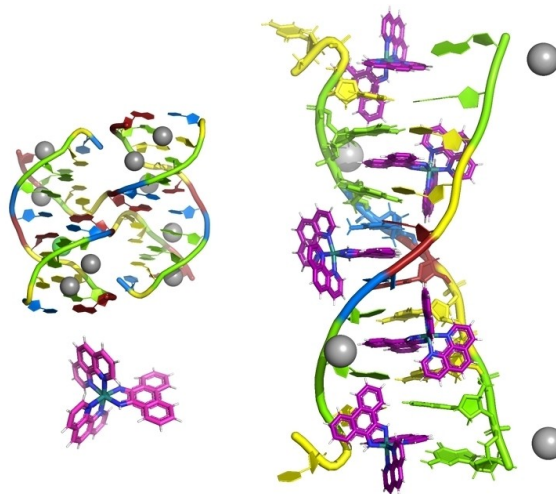
Research Articles

DNA Grooves

T. D. Prieto Otoya, K. T. McQuaid,
J. Hennessy, G. Menounou, A. Gibney,
N. G. Paterson, D. J. Cardin, A. Kellett,*
C. J. Cardin* ———————— e202318863

Probing a Major DNA Weakness: Resolving the Groove and Sequence Selectivity of the Diimine Complex Λ-[Ru(phen)2phi]2+

Major changes—the crystallisation of a junction forming DNA decamer with Λ-[Ru(phen)2phi]2+ shows three different sequence-selective binding modes, and displacement of Sr2+ from the minor groove to the interhelical space.